Experimental modelling of mantled porphyroclasts

CEES W. PASSCHIER*

Faculteit Aardwetenschappen, Rijksuniversiteit Utrecht, Budapestlaan 4, 3508 TA Utrecht, The Netherlands

and

DIMITRIOS SOKOUTIS

Hans Ramberg Tectonic Laboratory, Department of Mineralogy and Petrology, Institute of Geology,
Uppsala University, Box 555, S-75122 Uppsala, Sweden

Abstract—Mantled porphyroclasts are commonly used as sense of shear indicators in mylonites. Analogue experiments have been carried out to model the development of such objects. Rigid spheres mantled by a viscous Plasticene–putty mixture with power-law behaviour were suspended in an optically transparent Newtonian polymer matrix. The samples were deformed between two cylinders, one placed within the other, and with coinciding axes. This induces a non-coaxial flow between the cylinders and allows the achievement of high finite strain. The viscous mantle around the rigid sphere remained undeformed, deformed into an ellipsoid, or developed wings. The final geometry depends mainly on the induced viscosity contrast between the mantle and the matrix, which is a function of the flow-induced stress on the surface of the mantle. Winged mantles only develop if the induced viscosity contrast between the mantle and the matrix polymer is sufficiently small. If this 'critical' induced viscosity contrast is exceeded, the mantled sphere remains undeformed or obtains a stable ellipsoidal shape, even at high finite strain. δ-shaped winged mantles only develop in simple shear flow if the mantle around a rigid sphere is thin.

INTRODUCTION

MANY mylonitic rocks contain mantled porphyroclasts, i.e. aggregates (usually monomineralic) consisting of a relatively undeformed core and a deformed fine-grained, commonly recrystallized mantle (Hanmer & Passchier 1991) (Fig. 1). The core is usually equidimensional or ellipsoidal, while the mantle may be elongate with two distinct 'wings' stretching away from the core (Fig.1). Mantled porphyroclasts are also known as porphyroclast systems (Passchier & Simpson 1986) or rotating objects (Van den Driessche 1986) and are thought to develop by deformation of a mantle around a rigid core in response to flow in the surrounding matrix (Passchier & Simpson 1986). Common examples are coarse feldspar grains mantled by fine-grained recrystallized feldspar in quartz–feldspar mylonites (Tullis & Yund 1985, Passchier & Simpson 1986, Hooper & Hatcher 1988), carbonate nodules in deformed limestone (see the cover

---

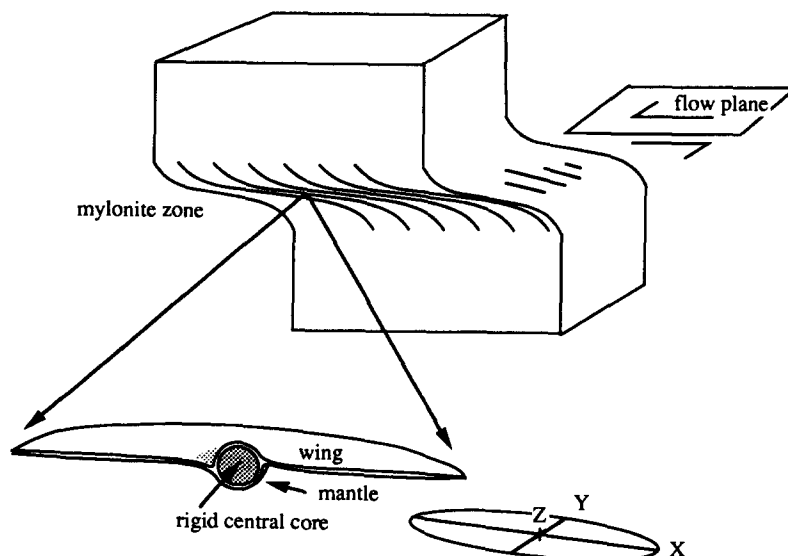*Present address: Department of Geology, University of Mainz, 55099 Mainz, Germany.

Fig. 1. Sketch of a mylonite zone with a deformed mantled porphyroclast. The orientation and geometry of the finite strain ellipse is shown at lower right.

of *Journal of Structural Geology*, Volume 12) and partly recrystallized pyroxene porphyroclasts in peridotite mylonites (Vissers *et al*. 1991).

In many cases, porphyroclast mantles are asymmetric (Fig. 1). This is thought to reflect the non-coaxial nature of progressive deformation in the matrix (Passchier & Simpson 1986). The asymmetry is most obvious in cross-section parallel to the *XZ*-plane of finite strain (Fig. 1) and such mantle-shapes can be used to determine sense of shear (Passchier & Simpson 1986).

Unfortunately, little is known about the mechanics of mantled porphyroclasts and the physical parameters that control their final geometry. Pioneering work was based on microstructural observations and on two-dimensional analogue experiments deforming 'passive marker' mantles around rigid cylinders (Passchier & Simpson 1986, Van den Driessche 1986, Van den Driessche & Brun 1987). The experimental approach is extended here to deformation of 'mantled spheres', i.e. aggregates of a rigid sphere with a mantle of a viscous material in an optically transparent polymer matrix (Fig. 2). The transparent matrix material, which was exhaustively described by Weijermars (1986a,b,c), allows three-dimensional monitoring of the deformation of the mantle. Although the rheology of our model materials differs from that of rock forming minerals, the use of different mantle and matrix material is more realistic than the use of a passive marker mantle as in earlier experiments.

MATERIALS AND METHODS

The experiments were carried out in a coaxial-cylinder viscometer (Hailemariam 1982) in which high shear strain values (up to $\gamma_c = 120$; see Table A1 in the Appendix) can be reached without loss of cohesion in the sample (Fig. 2). This is necessary because some geometries of mantled porphyroclasts can only be modelled at finite strain values exceeding $\gamma = 3$, the limit attainable in most conventional shear-boxes (Passchier & Simpson 1986, Van Den Driessche & Brun 1987). The viscometer was filled with a transparent polymer in which a mantled rigid sphere was embedded (Fig. 2). The experimental materials were deformed in creep between a fixed outer cylinder and a rotating inner cylinder, driven by suspension of a weight from an attached rotor (Fig. 2a). The procedure is outlined in detail below.

Figure 3 illustrates the rheological properties of the experimental materials. Since logarithmic axes are used for shear stress (log τ) and engineering strain rate (log $\dot{\gamma}$), the inverse of the slope of the curves in Fig. 3 equals the power-law exponent n of the constitutive equation. Materials are either Newtonian ($n = 1$) or strain rate softening ($n > 1$). n values between 1 and 10 have been found for rocks and minerals during experimental deformation in the solid state (cf. Carter 1975, 1976, Tullis 1979, Kirby 1983). The transparent matrix material used in our experiments is a polymer, polydimethyl-siloxane

(PDMS). We used a PDMS manufactured by Dow Corning of Great Britain under the trade name SGM 36 (Weijermars 1986a,b,c). Throughout this paper, the abbreviation PDMS refers specifically to this material. Its flow behaviour is Newtonian ($n = 1$; viscosity 5×10^4 Pa s) at low differential stresses but shows a transition towards strain rate softening at differential stress values exceeding 1000 Pa. (Weijermars 1986a,b,c)(Fig. 3).

Five different materials a–e were used for the mantle of the rigid sphere in the experiment (Table 1). They are mixtures of two basic materials: Rhodorsil Gomme (a) and Plastilina (e). Rhodorsil Gomme GSIR is a pink opaque bouncing putty supplied by the Société des Chemiques Rhône-Poulenc (France). It is a Newtonian material with a viscosity of 2.9×10^4 Pa s (Hailemariam
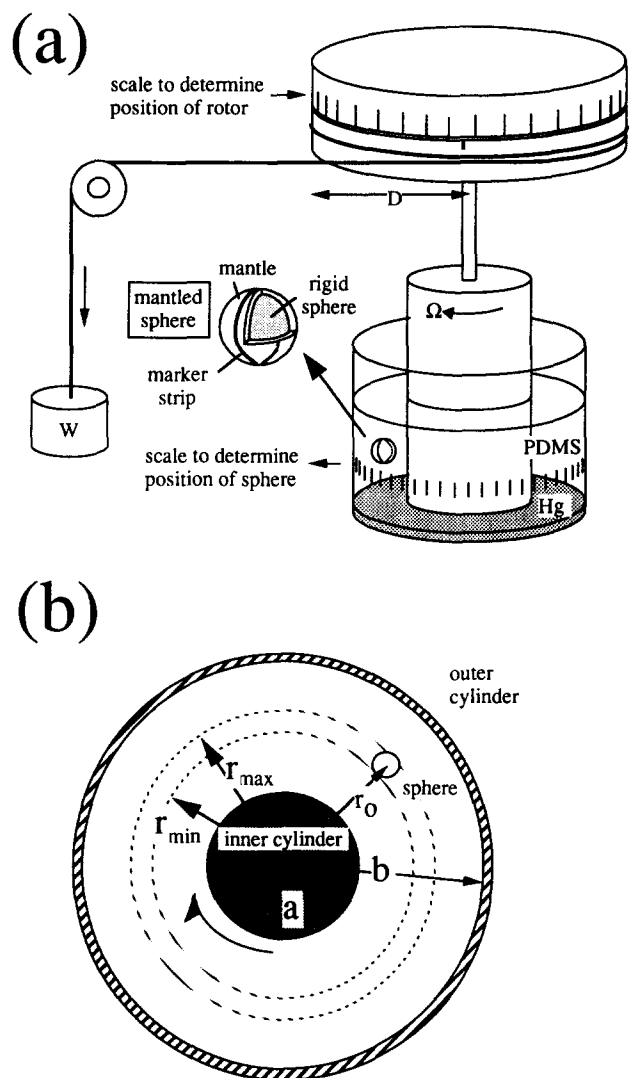
Fig. 2. Sketch of the experimental set-up. (a) Viscometer in which the experiments were carried out. The apparatus consists of a fixed transparent outer cylinder and an inner cylinder which is free to rotate. The inner cylinder is driven by a weight suspended from a rotor. The metal frame supporting the rotor and the outer cylinder has been omitted from the drawing for clarity. The space between the cylinders is filled with a mercury (Hg) layer and a transparent matrix material (PDMS). A rigid sphere mantled by a thin layer of deformable mantle is inserted in the PDMS matrix, and both are deformed by non-coaxial flow in response to the movement of the inner cylinder. (b) Cross-section through outer and inner cylinder showing the position of the mantled sphere in the PDMS matrix. h, W, D and Ω and other parameters are explained in the Appendix.
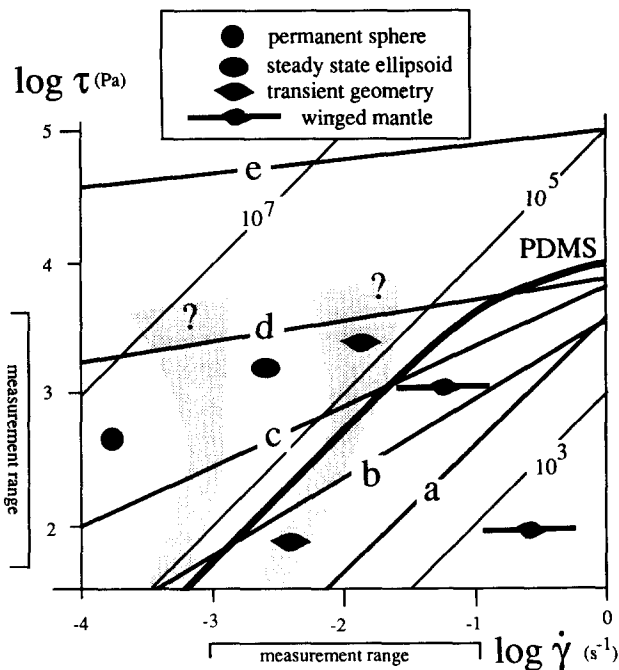
Fig. 3. Shear stress (τ)–shear strain rate ($\dot{\gamma}$) diagram. Bold lines—flow curves for the materials used in the experiments. Thin diagonal lines—viscosity contours in Pa s. Shaded fields—boundaries between categories of mantle shape as determined during experiments and projected from Fig. 10. PDMS—Polydimethyl-siloxane (PDMS), the matrix material used in the experiments; a–e—mixtures of Plastilina (e) and Rhodorsil Gomme (a) used as mantle materials. The range of shear strain rate and shear stress values attainable in our experiments is indicated. Further explanation in text.

same material using a coaxial-cylinder (Couette) viscometer as shown in Fig. 2. The viscosities of materials **b** and **c** were measured in the coaxial-cylinder viscometer.

Thirty-five experiments have been carried out with three different sizes of inner (a) and outer (b) cylinder parts (Fig. 2b: $a = 0.03$ m and $b = 0.04$ m; $a = 0.02$ m and $b = 0.04$ m; $a = 0.01$ m and $b = 0.018$ m), three sizes of rigid spheres (2, 4 and 6 mm diameter) and variable mantle composition and width. The reason for this variation is, that the desired range of stress values (between 50 and 8000 Pa) and strain rates (between 0.001 and 0.1 s^{-1}) in PDMS could only be obtained in this way. In order to avoid boundary effects, the size of the rigid spheres had to be adapted to the width of the specimen chamber; spheres with a diameter of 0.2–0.3 times the width of the specimen chamber have been used throughout.

Experimental set-up

For each experiment the space between the inner and outer cylinder of the viscometer was filled with 5 mm of mercury, and up to 50 mm of PDMS (Fig. 2a). The viscometer and its content were then centrifuged for 10 min at 1000 g to remove air bubbles. After centrifuging, the inner cylinder and a clear bubble-free PDMS float freely on the mercury-layer (Fig. 2a). Friction of the inner cylinder and the PDMS with the bottom of the viscometer can therefore be neglected.

Rigid spheres of 2–6 mm diameter with a density close to that of PDMS were covered by a mantle of one of the materials **a–e** with a thickness of 0.5–1 mm (Fig. 2a). Two perpendicular great circle marker strips of coloured mantle material (Fig. 2a) were placed approximately perpendicular to each other in the mantle. These marker strips allow reconstruction of the change in shape of the mantle, but do not affect mantle behaviour; they are composed of the same material as the rest of the mantle and independent tests have shown that the pigment used does not affect the rheology. After air bubbles were removed from the PDMS matrix by centrifuging, a cylindrical hole was opened in the PDMS in order to insert the mantled sphere in the centre of the PDMS layer. The whole system was then left for approximately 2 h during which the cylindrical cavity above the inserted sphere closes by gravitational flow of PDMS. After some experimentation, this results in a mantled sphere in PDMS with only a few minor bubbles around and above the object.

1982, Weijermars 1986a). Plastilina is the Swedish version of Harbutt's Plasticine (McClay 1976). It is highly non-Newtonian with a power-law exponent $n = 9.5$ (McClay 1976). A Newtonian silicone bouncing putty becomes non-Newtonian after mixing with Plastilina as the concentration of solid particles increases (Onogi & Matsumoto 1981, Weijermars 1986a). The mixtures are therefore all non-Newtonian and close to 'power-law' flow with n values between 1.5 and 7.1 (Table 1 and Fig. 3). The rheological properties of all the mixtures are accurately known and have been determined for several temperatures by Weijermars (1986a), Koyi (1988) and Treagus & Sokoutis (1992). Viscosity measurements of PDMS and materials **d** and **e** were done at 24°C (Weijermars 1986a,b,c). Measurements of materials **a**, **b** and **c** were done at 18, 30 and 42°C (Koyi 1988) and the position of the curves for 24°C were calculated (Fig. 3). The flow curves for PDMS and materials **a**, **d** and **e** (Fig. 3) were determined using a West German 'Haake' capillary steady-state extrusion viscometer. These curves were closely matched by other curves for the

Experimental procedure

After sample preparation was completed, the upper part of the viscometer, the rotor, was put into place and attached to the inner cylinder (Fig. 2a). A weight was then suspended from the rotor, starting the experiment. During each experiment, the following parameters were monitored (Fig. 2a);

(a) rotation angle on the rotor, from which bulk finite shear strain is calculated;

Table 1

Material	Weight % Rhodorsil Gomme	Weight % Plastilina	n value
a	100	0	1
b	68	32	1.5
c	45	55	2.2
d	32	68	7.1
e	0	100	9.5

(b) angular velocity of the rotor and inner cylinder (bulk strain rate);

(c) position of the centre of the deforming mantled sphere with respect to the fixed outer cylinder; this information is needed to determine the distance of the object from the central axis of the viscometer.

Experiments lasted from 5 min to several hours, depending on the imposed bulk strain rate. Most experiments were interrupted, and consist of several legs. At least after two revolutions of the inner cylinder (γ_c = 30–50) the experiment had to be stopped to rewind the rope on the rotor from which the weight is suspended. Also, some experiments were interrupted to increase the weight suspended from the rotor in order to investigate the effect on the deforming mantle, or to take photographs. Experimental data show that the angular velocity of the inner cylinder increases during the first 10 s of a deformation leg, after which it stabilizes for the rest of the leg for up to two full revolutions of the inner cylinder; our observations are made during this steady-state part of the leg. Both the externally applied stress and strain rate in PDMS were therefore constant during

individual legs of each experiment. The geometric development of the mantled porphyroclast was monitored by a series of photographs made at regular intervals during the experiments.

OBSERVED GEOMETRIES FOR MANTLED SPHERES

Thirty-five experiments were carried out at different angular velocity of the inner cylinder, and for different mantle materials and initial mantle thickness. Four main classes of mantled sphere geometry have been observed during our experiments (Fig. 4a). These are: (1) permanent sphere; (2) steady-state ellipsoid; (3) transient geometries; and (4) winged mantles.

Permanent sphere

Some mantled spheres show rigid-body rotation behaviour; they do not change shape, and marker lines on the surface of the body have constant angular velocity in
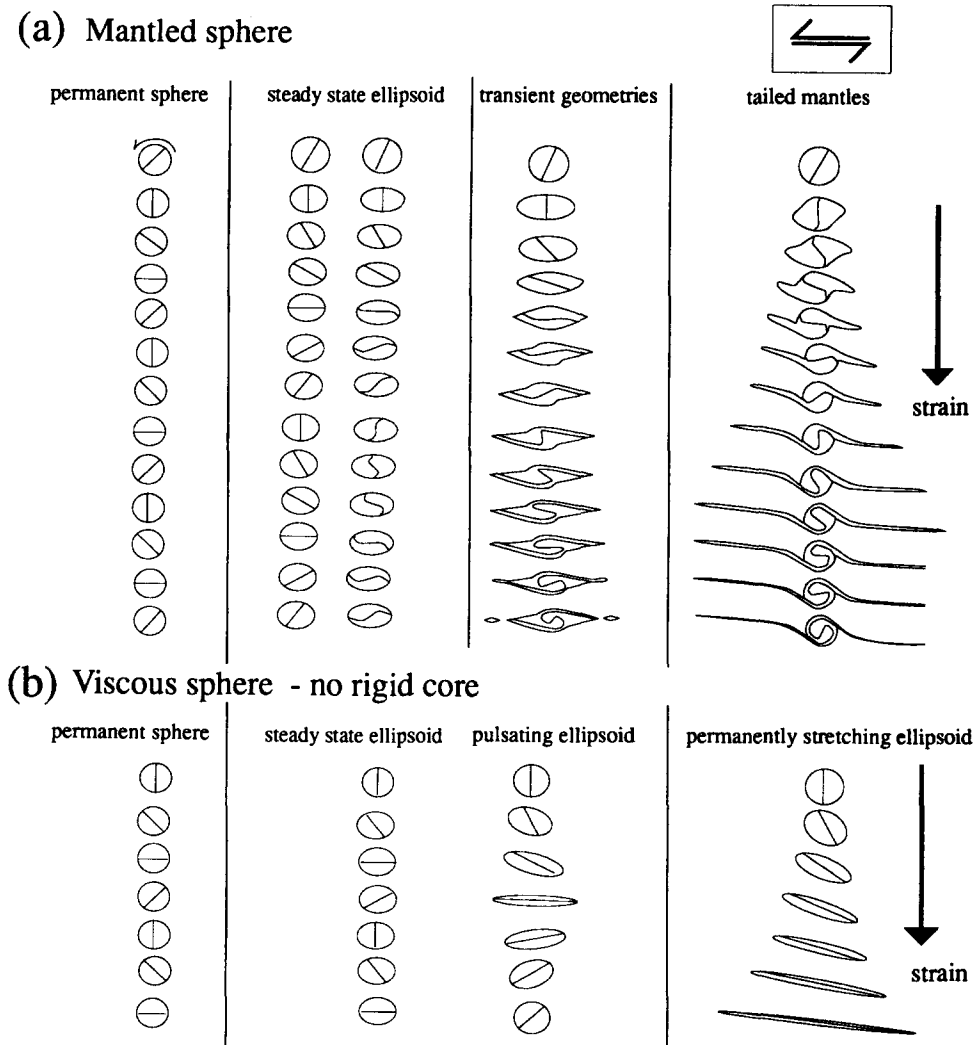

Fig. 4. (a) Diagram showing the four main classes of mantle geometry observed during the experiments. Objects are shown as observed from the Y-strain axis direction (in the experiment; from the top of the viscometer). Lines on mantled spheres are marker lines to show the effect of rotation and internal deformation. (b) Geometries observed in viscous spheres which lack a rigid core for similar mantle materials. Finite strain is increasing downward, but is not of equal scale for different categories.

a matrix deforming by steady-state flow (Fig. 4a). Such 'permanent spheres' rotate with an angular velocity of half the shear strain rate, as predicted by theory (Jeffery 1923). In some cases, minor sheath fold-type lobes develop on the sides of the mantle parallel to the shear zone surface. These lobes remain 'plastered' against the mantled sphere and do not develop into permanent wings. Notice that this rigid-body rotation is observed for spheres with mantles of a deformable material.

Steady-state ellipsoid

Some mantled spheres deform into a 'steady-state ellipsoid' with small aspect ratio ($R < 1.4$) which remains oriented with its long axis at a small angle to the surface of the outer cylinder (Figs. 4a and 5). The exact orientation cannot be determined at this small aspect ratio. The external shape and orientation of the mantle does not change notably with progressive deformation (Fig. 4a). Marker lines on ellipsoids with small aspect ratio remain straight, circle round the mantled sphere during progressive deformation and are periodically shortened and elongated (Fig. 4a, second column and Fig. 5). If the aspect ratio of the steady-state ellipsoid approaches $R = 1.4$, marker lines on the mantle do not remain straight; where the marker line rotates into the tips of the ellipsoid, it becomes 'retarded' with respect to the top and bottom part, resulting in a folded marker line (Fig. 4a, third column).

Transient geometries

Mantled spheres with a transient geometry show a cyclic change in shape, contrary to the permanent sphere and steady-state ellipsoid classes of behaviour. If a developing ellipsoid slightly exceeds $R = 1.4$, the 'wings' of the ellipsoid are not affected by a rotation of the central rigid sphere; as a result, material is retarded here, and marker lines on the mantle are folded, as described above. With progressive deformation the ellipsoid is modified to a spindle-shaped aggregate with a characteristic asymmetric 'indented' shape (Figs. 4a and 7a). If the mantle of the sphere is wide the shape can be relatively stable, but in other cases it may fold inwards and a wing will start to form at high bulk strain values. This wing will boudinage and detach from the mantled sphere, after which an asymmetric indented shape develops anew. The result is a spindle-shaped aggregate from which wings detach periodically. The asymmetry of the indented shape is weak (Fig. 7a) and is present only part of the time, while for most of the time the mantled sphere is symmetric.

Winged mantles

Winged mantles consist of a central mantle relict around the rigid sphere, and two wings of mantle material that stretch into the PDMS matrix. The length to these wings is a function of finite strain (Fig. 4a). We distinguish three major types of winged mantles depend-

ing on the width of the developing wings in the Y-direction; ridged, sheathed and coiled mantles (Fig. 9). Ridged mantles develop wings with a width in the Y-direction equal to the diameter of the original spherical mantle. As a result, 'ridges' form alongside the rigid sphere (Figs. 6, 7b and 9). Sheathed mantles have wings of the same width as the rigid sphere and lack ridges in the Y-direction; the mantle sheds two sheaths of material which stretch laterally into wings (Figs. 8 and 9). Coiled mantles have thin wings which may be cylindrical in cross-section. These wings may 'coil' around the mantled sphere and tend to neck and boudinage (Figs. 7g–j and 9). The width of wings in the Y-direction depends on mantle rheology. Coiled mantles develop in more viscous material (d), while at lower viscosities (a–c) sheathed, or ridged mantled spheres form (Fig. 9).

Secondary wings form commonly for sheathed and coiled mantles (Fig. 8c). Variations in strain rate seem to enhance development of such new wings. The geometry of wings in coiled and sheathed mantles is less regular than for ridged ones: the tip of a wing tends to remain wider than the central part of the wing in response to necking (Figs. 7f & g). As a result, the end section may start to rotate independently from the parent porphyroclast (Fig. 7g).

All three categories of winged mantles may develop embayments near the rigid sphere, as shown in Fig. 9. In cross-section parallel to the XZ plane, these mantles show a pronounced δ-shape asymmetry (δ-shape wings; Passchier & Simpson 1986) (Figs. 7b & c, 8 and 9). Alternatively, embayments may be absent, in which case the mantle has an approximately symmetric shape in XZ cross-section (Figs. 6, 7d & j and 9; symmetric wings). Intermediate geometries also occur, where mantles are indented but do not develop real embayments.

For coiled mantles, asymmetric indented shapes are more common than real δ-shapes (Figs. 7e–j). The shape of the deformed mantle is usually highly unstable, and new wings develop at regular intervals (Figs. 7f–j). Wings that develop on mantles with a high n value tend to boudinage, which is in agreement with material behaviour predicted by Smith (1977). As a result, the mantled sphere periodically looks like a little deformed object after old wings have just been shed and before new ones start to form, even at high strain (Fig. 7h).

Observed geometry for viscous spheres

In a number of experiments, massive viscous spheres of mantle material were tested to study the effect of the absence of a rigid spherical core (Fig. 4b). The series is not complete, and we can only give an indication of the possible range of behaviour. With increasing strain rate in the PDMS matrix and decreasing n value of mantle material, the following change in behaviour has been observed.

As for mantled spheres, viscous spheres can remain undeformed for low strain rate and high n value. Where mantled spheres show steady-state ellipsoid and transient behaviour, viscous spheres develop into steady-

state or 'pulsating' ellipsoids (Fig. 4b). A pulsating ellipsoid (Ramberg 1975, Pfiffner & Ramsay 1982) stretches and rotates towards the flow plane; rotates through the flow plane and shortens to (or nearly to) a sphere, and starts deforming anew (Fig. 4b). However, if the maximum aspect ratio exceeds a value of approximately $R = 5$, the ellipsoid tends to buckle rather than to shorten and may obtain an irregular shape from which fragments or wings are shed. At conditions where permanent wings are formed for mantled porphyroclasts, viscous spheres deform into permanently stretching ellipsoids which gradually rotate towards the flow plane (Fig. 4b). At low n values the ellipsoid stretches as a passive (strain) ellipsoid, but at high n values it is constricted in the Y-direction and tends to boudinage.

Our results on viscous spheres are similar to those of Taylor (1934), Rallison (1984) and Bentley & Leal (1986) who did experimental work on deformation of oil drops. They found that Newtonian viscous inclusions in a less viscous matrix with a viscosity contrast of more than 4 remain undeformed at all strain rates in simple shear (Taylor 1934, Rallison 1984, Bentley & Leal 1986). At smaller viscosity contrast the behaviour of viscous inclusions depends on strain rate in the matrix. At low strain rate steady-state ellipsoids are formed. The steady state is commonly reached through an intermediate state as a pulsating ellipsoid. Beyond a certain strain rate, a viscous inclusion may start to deform permanently (Taylor 1934, Rallison 1984, Bentley & Leal 1986). It is difficult to compare results quantitatively, however, because of the non-Newtonian character of our materials and insufficient accuracy of measurements in our set-up.

EXPERIMENTAL CONDITIONS FOR OBSERVED GEOMETRIES

In order to determine which factors influence the geometry of deformed mantles, the results of different experiments must be compared in some way. Angular velocity of the inner cylinder is unsuitable for this purpose, since cylinders of different diameter were used, and since the behaviour of a mantled sphere is dependent on its radial position in the viscometer. We have therefore chosen to compare experimental results using the inferred shear stress τ at the position of the mantled sphere in the PDMS during the experiment. τ at a radius r in PDMS in the viscometer is given by (see Table A1 in the Appendix)

$$\tau = \frac{(W - m')gD}{2\pi h r^2}. \tag{1}$$

Since shear stress is a function of r, we give for each experiment the inferred shear stress range between the radii corresponding to the apices on the mantled sphere nearest to the inner (τ_i) and outer (τ_e) cylinder, respectively (Fig. 2b). These limits are given as (see Table A1 in the Appendix)

$$\tau_i = \tau\{r_{min}\}; \qquad r_{min} = r_o - d/2 \tag{2a}$$

and

$$\tau_e = \tau\{r_{max}\}; \qquad r_{max} = r_o + d/2. \tag{2b}$$

r_o, the position of the centre of the sphere, is calculated from the angular velocity (ω) of the mantled sphere with respect to the angular velocity of the inner cylinder (Ω) using

$$r_o = \sqrt{\frac{\Omega b^2 a^2}{\omega(b^2 - a^2) + \Omega a^2}}. \tag{3}$$

Notice that τ_i and τ_e are inferred stress values in PDMS away from a mantled sphere and not actual values in the mantle.

Figure 10 is a plot of inferred stress value range for all experiments. Since the experimental set-up only allows realization of shear strain rates in the PDMS matrix of 10^{-3}–10^{-1} s^{-1}, a stress window of 50–8000 Pa could be covered during the experiments (Fig. 3). It is clear from Fig. 10 that certain mantle geometries develop at specific stress levels for each mantle material. This was evident in single experiments when applied stresses were gradually increased. The stress values of boundaries between geometry classes in Fig. 10 have been plotted for each material on the flow curves in Fig. 3, to see how geometry classes are distributed. Shaded contours give the boundaries between the main geometry classes of mantled objects.

There is also a dependence of winged mantle shape on mantle thickness (Fig. 10). For thin mantles, δ-shape wings develop; for wide mantles, symmetric wings form. A weak tendency exists for boundaries between categories to move to higher stress levels for thinner mantles (Fig. 10, material **d**). This effect could not be expressed quantitatively, however. We found that the effect of mantle width was most pronounced for mantle thickness less than 20% of the radius of the rigid sphere. The boundaries between shape categories shown in Fig. 3 are for relative mantle widths of 0.3–0.8.

DISCUSSION OF EXPERIMENTAL RESULTS

The dependence of mantle geometry on shear stress in the matrix (Figs. 3 and 10) can be explained as follows. For non-Newtonian materials as used in our experiments, the viscosity of the mantle depends on the flow-induced stress field on the mantle surface. An increase in strain rate in PDMS will raise the magnitude of these flow-induced stresses and thereby the strain rate in the mantle material. Since the flow curves of most mantle materials are less steep than that of PDMS (Fig. 3) the strain rate in these mantles will increase more rapidly than in PDMS, effectively lowering the viscosity contrast between mantle and matrix. The fact that the geometry of a mantled sphere can be changed by changing differential stress in PDMS is therefore interpreted to mean that mantle geometry mainly depends on the induced viscosity contrast. The radial stress gradient in
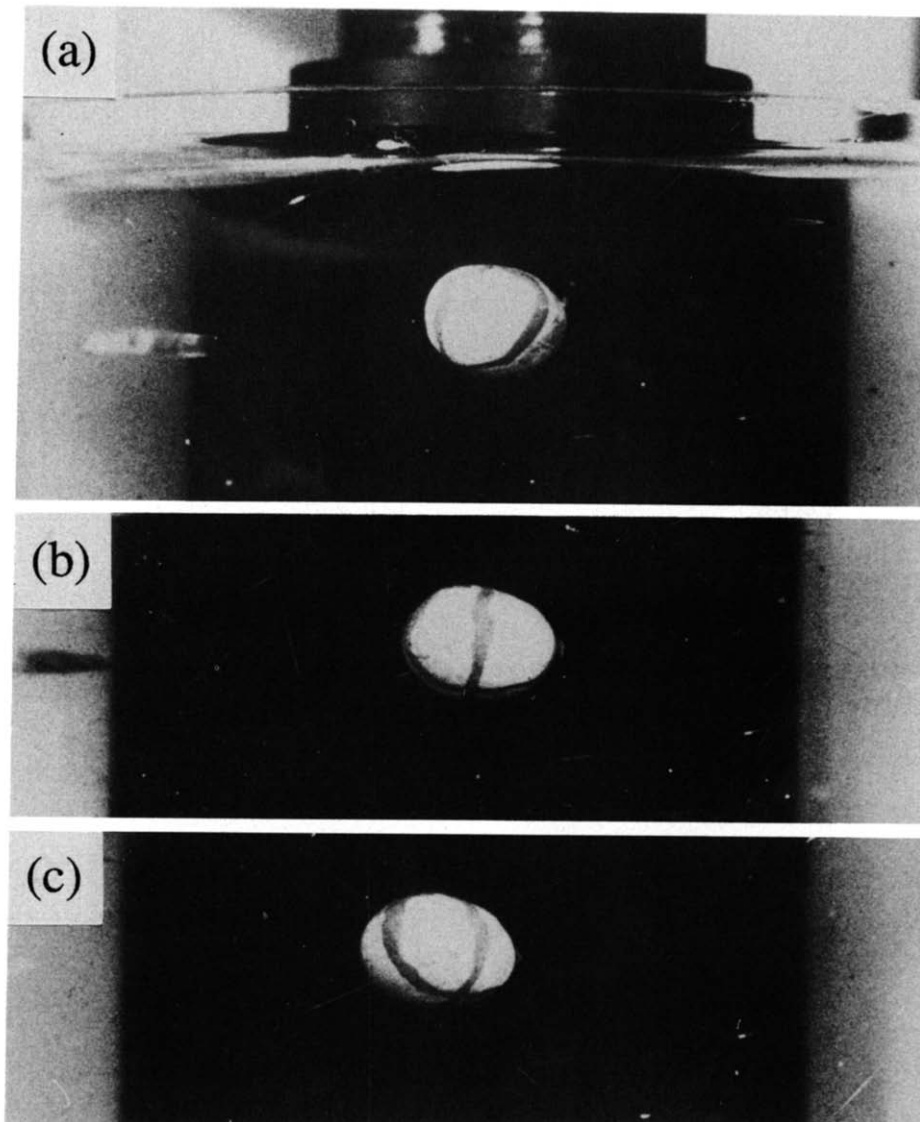
Fig. 5. Steady-state ellipsoidal mantle developed in material c as visible through the outer cylinder wall during three stages of an experiment. The inner cylinder seen at the background rotates to the left. Shear strain between steps (a)–(c) is 4. The Y-axis of finite strain is vertical and parallel to the paper in this view. The two marker lines in the mantle were orthogonal great circles on the original sphere. The same marker line appears at left in (a), in the centre in (b), and at right in (c).
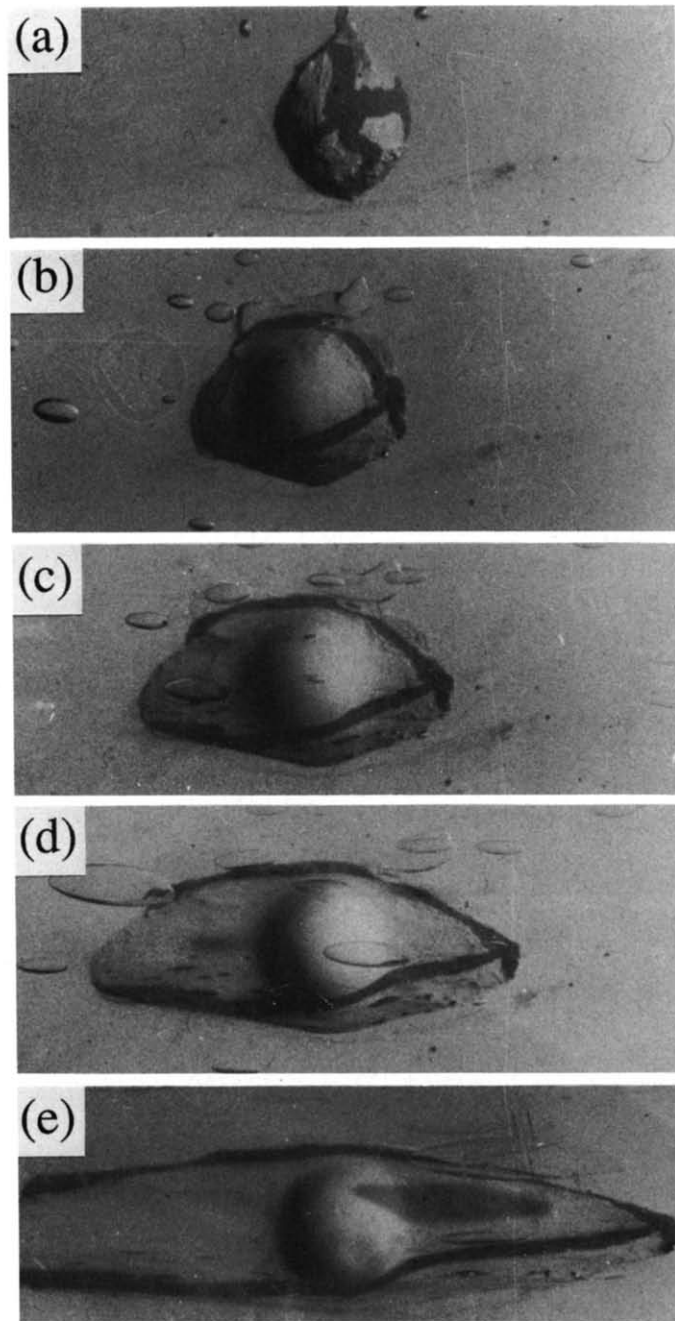
C. W. Passchier and D. Sokoutis

Fig. 6. Five stages in the development of a ridged mantle in material a. Front moves to the right and Y-axis is vertical in the plane of the paper. (a) Undeformed mantle. (b)–(e) The mantle stretches into a ridged mantle maintaining its initial width in the Y-direction. Because of the initially wide mantle, the winged mantle remains symmetrical and does not develop a δ-shape. Notice the ellipsoidal shape of gas bubbles in deformed PDMS. (a) $\gamma_c = 0$. (b) $\gamma_c = 2.7$. (c) $\gamma_c = 4.9$. (d) $\gamma_c = 9.8$. (e) $\gamma_c = 13.4$.
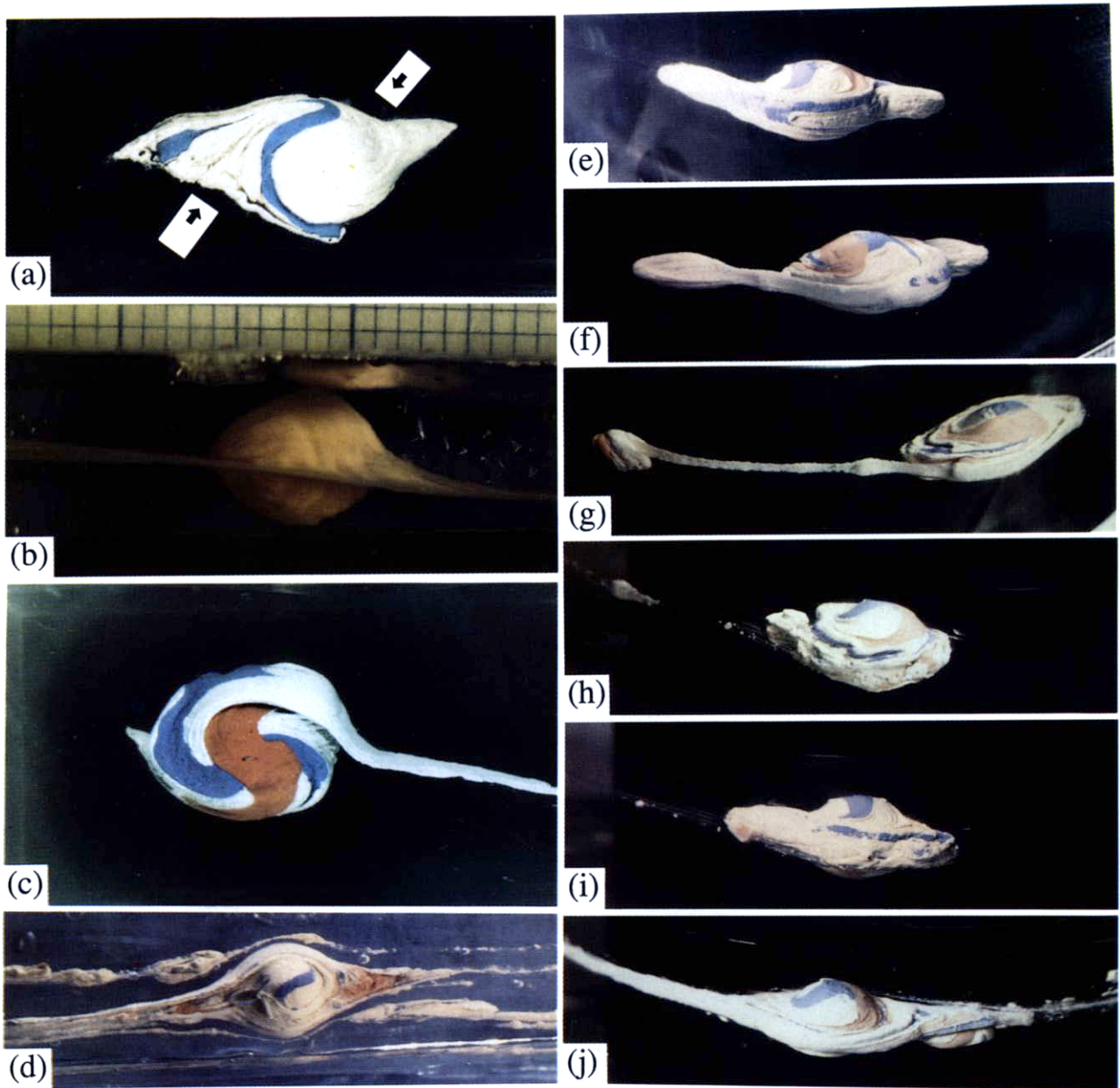
Fig. 7. (a)–(d) Deformed mantles as observed from the Y-strain axis direction (in the experiment; from the top of the viscometer). The objects were taken out of the viscometer for photography. Folded marker lines were great circles on the initial mantle. (a) Spindle-shaped mantle with transient geometry in material d, $\gamma_c = 150$. Dextral shear sense. (b) Ridged mantle in material a, δ-shaped in cross-section. $\gamma_c = 14$. Sinistral shear sense. (c) Coiled mantle with δ-shape wings in material c, observed oblique to the Y-axis. $\gamma_c = 53$. Sinistral shear sense. (d) Coiled mantle with symmetric wings in material d after $\gamma_c = 110$. Remnants of a deflected blue marker line are visible in the little-deformed central part of the mantle. Dextral shear sense. Strips of material to the sides of the mantled sphere are parts of the wing which had spiralled round the viscometer and reappeared on the inner and outer side of the mantled sphere. (e)–(j) Stages in the development of the geometry of the coiled mantle in (d) (material d), observed from a direction in the YZ-plane at 30° from the Z-axis. Sinistral shear sense. (e) Indented shape with incipient wings. Marker lines are deflected. $\gamma_c = 51$. (f) Wing at left starts to boudinage. $\gamma_c = 56$. (g) Boudinaged tip of one of the wings starts to rotate as an independent new object. The relic mantled sphere is nearly separated from its wing. $\gamma_c = 66$. (h) Wing is completely detached and an ellipsoidal, symmetric mantle remains. At left, relics of a boudinaged wing are just visible. $\gamma_c = 75$. (i) Mantle develops again into an indented shape as (e). $\gamma_c = 84$. (j) Symmetric coiled mantle in a final stage of the experiment. $\gamma_c = 90$.
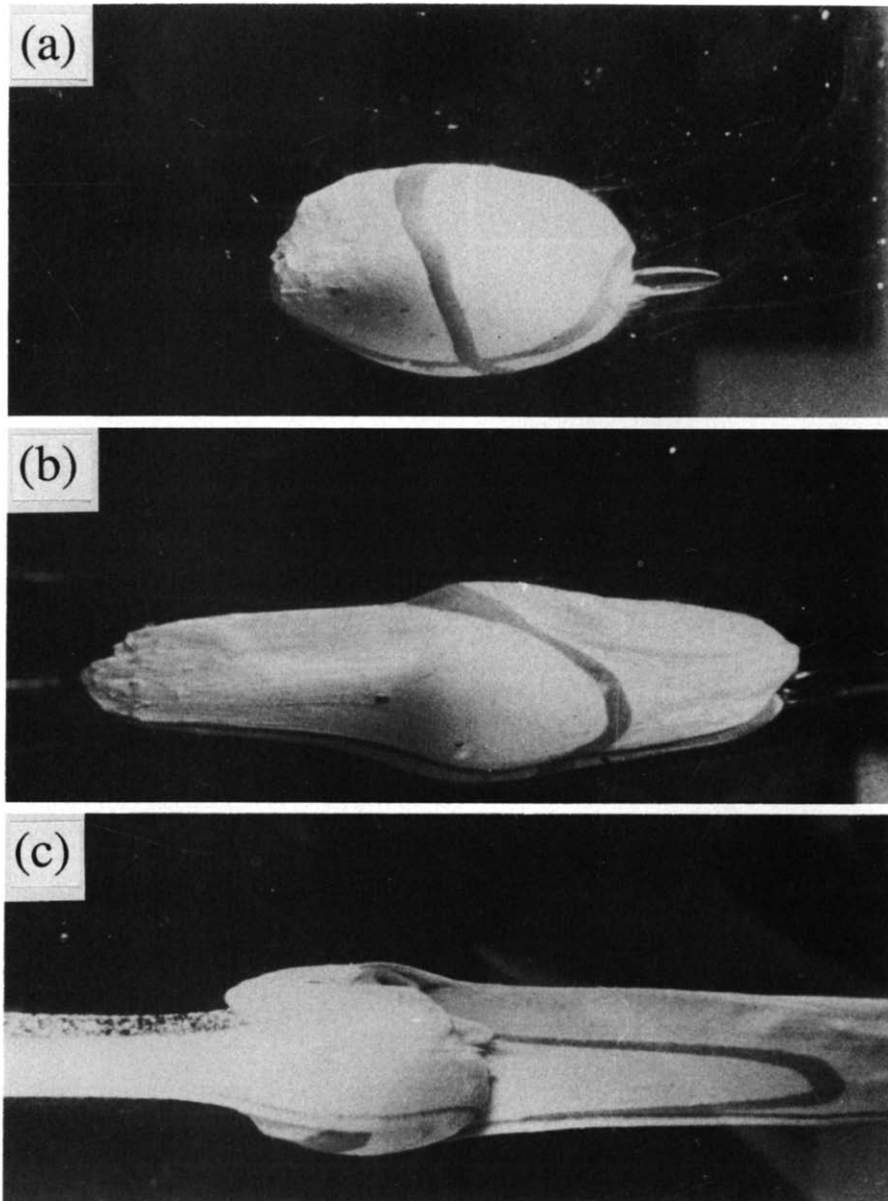
Fig. 8. Three stages in the development of a sheathed mantle in material **c**. Front moves to the right. Y-axis is vertical in the plane of the paper. (a) Spindle-shaped ellipsoidal mantle. $\gamma_c = 9$. (b) Indented shape develops. $\gamma_c = 19$. The central marker line in (a) has now rotated to the indentation in the wing at right. (c) Fully developed coiled mantle with δ-shape wings. $\gamma_c = 36$. One of the embayments is visible at right of the central sphere; an incipient secondary wing is seen to develop in the top section of the embayment. The folded marker line in the wing on the right is the same line that was in a central position at (a); another sector of the same marker line is visible at the lower and upper side of the coiled left-hand wing in the central part of the mantled sphere. The wing at the left is starting to boudinage and has become transparent near the top.
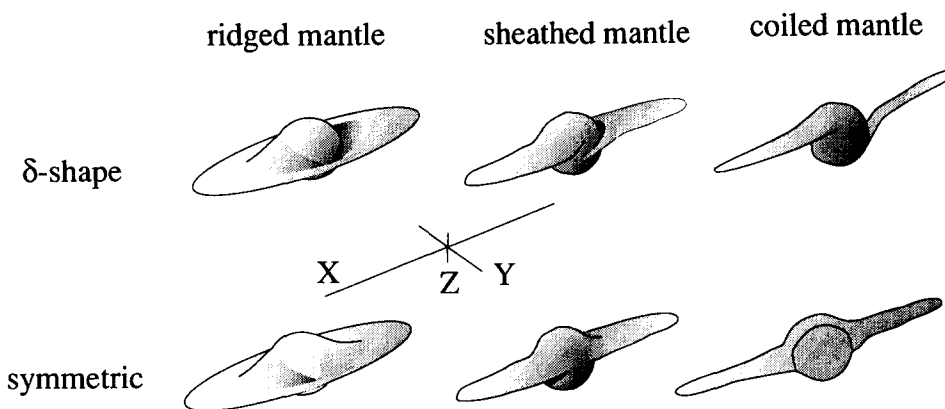
ridged mantle   sheathed mantle   coiled mantle

δ-shape

X   Z Y

symmetric

Fig. 9. Schematic drawing of the three categories of rigid spheres with winged mantles as observed during the experiments, both with δ-shape and symmetric shape.

PDMS also influences the induced viscosity in the mantle. This effect is illustrated in our experiments by the fact that wings which develop on the inner side of the viscometer are always longer and better developed than those on the outer side (Figs. 7a,c & f).

In the oil drop experiments of Taylor (1934), Rallison (1984) and Bentley & Leal (1986) a change in geometry of the drops with increasing strain rate is attributed to a competition of interfacial tension and flow-induced stresses on the surface. Data by Weijermars (1986b) and

theoretical considerations suggest that in our experiments interfacial tension between mantle and matrix is negligible compared to flow-induced stresses. Another factor must therefore be responsible for the affixation of material to rigid spheres at small flow-induced stresses. We propose that vortical flow-perturbations around a rigid sphere may be responsible.

The presence of a rigid sphere in a simple shear flow gives rise to a local flow-perturbation which is characterized by closed ellipsoidal streamlines near to the sphere

τ (Pa)   material d   material c   material b   material a

δ-shaped winged mantle
σ-shaped winged mantle
transient shape
steady state ellipsoid
permanent sphere

0.2 0.4 0.6 0.8   0.2 0.4 0.6 0.8   0.2 0.4 0.6 0.8   0.2 0.4 0.6 0.8
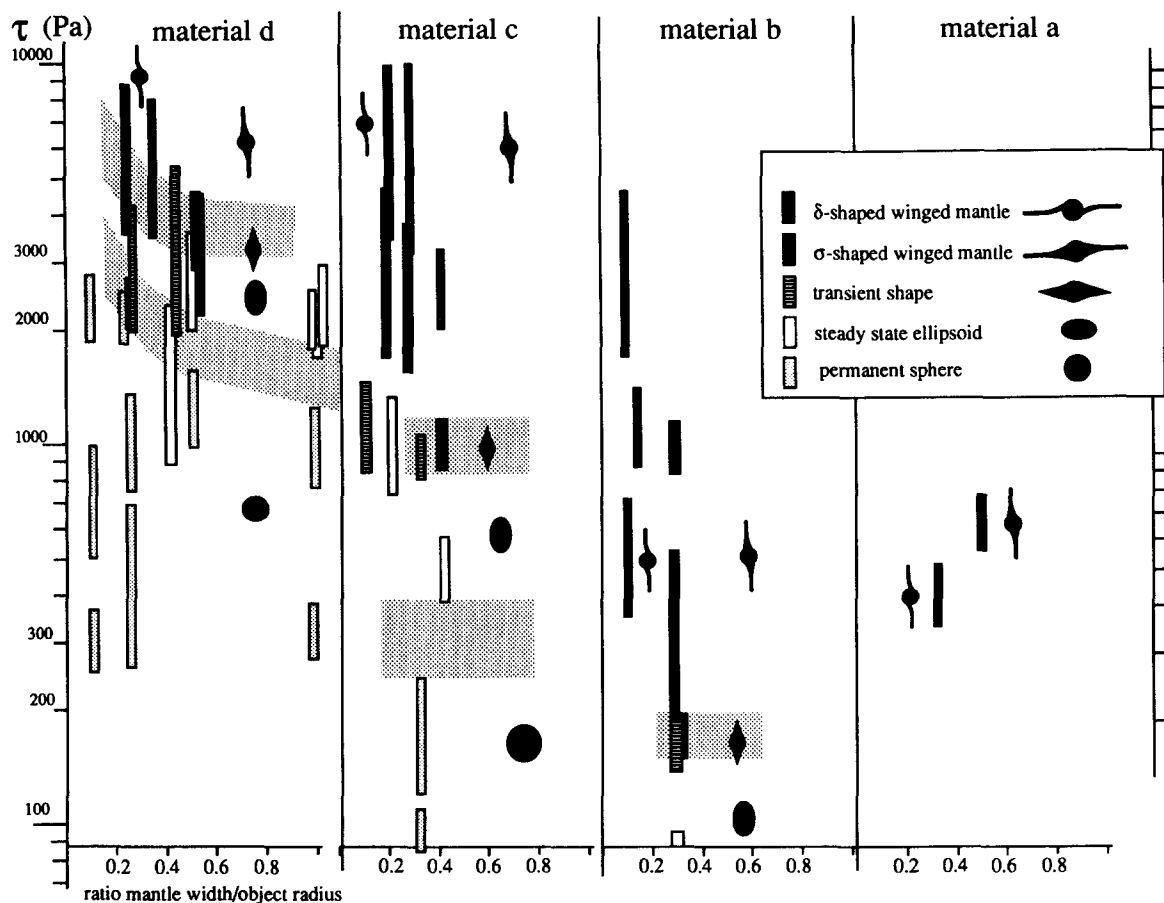
ratio mantle width/object radius

Fig. 10. Graph showing bars which represent the range of inferred shear stress values in PDMS at radii corresponding to the inner and outer apices of mantled porphyroclasts. All experimental results are plotted in this graph. Different geometry categories are indicated with different symbols and ornamentation on bars. For each material, the horizontal position of bars indicates the ratio of mantle width to mantled sphere radius at the start of the experiment. Shaded zones indicate the approximate boundaries between geometry categories.
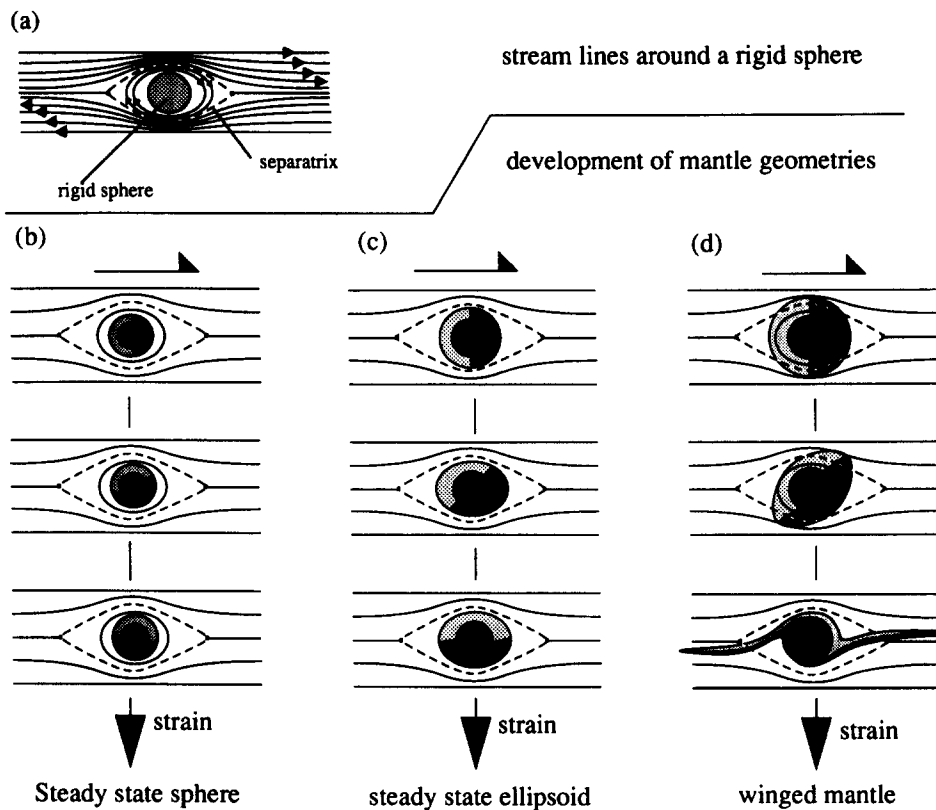
Fig. 11. Explanation of the dependence of the geometry of mantled spheres on mantle rheology. (a) Flow pattern showing streamlines around a sphere in a bulk simple shear flow, following Masuda & Ando (1988). The dashed line indicates the separatrix. (b)–(d) Three stages of progressive development of mantle geometry for three different types of mantle behaviour. For clarity, the mantle has been separated into two differently marked hemispheres. Solid lines indicate streamline pattern at the end of each stage. (a) At high viscosity contrast the mantle does not deform (permanent sphere). (b) At lower viscosity contrast local increase or decrease of angular velocity of mantle material creates a steady-state ellipsoid that remains inside the separatrix. (c) At low viscosity contrast, the mantle lies only partly within the separatrix. Consequently, the mantle is divided into a part forming wings with progressive deformation and a part which remains adjacent to the rigid mantled sphere; winged objects develop.

and open curved streamlines further away which grade into the straight streamlines of simple shear (Fig. 11a) (Masuda & Ando 1988). The pattern of streamlines resembles that of a so-called 'Kelvin cat's-eye' pattern in Kelvin–Helmholtz flow instabilities (cf. Ottino 1989, Kundu 1990, Meiburg & Newton 1991). The boundary separating open and closed streamlines can be called a *separatrix* after the terminology used to describe such patterns (Ottino 1989, Kundu 1990). Material inside the separatrix is permanently affixed to the rigid sphere if the separatrix does not change shape with time, while material outside the separatrix can move permanently away form the rigid sphere (Fig. 11).

A rigid sphere rotates at an angular velocity of up to half the shear strain rate of the matrix flow (Jeffery 1923). If the induced viscosity contrast between mantle material and matrix is high, the strain rates induced in the mantle may be negligible compared to the angular velocity of the rigid sphere, and the mantle does not change shape visibly; the mantled sphere lies within the separatrix and effectively rotates as a rigid object (permanent sphere; Figs. 4a and 11b).

If the induced viscosity contrast is smaller, strain rates induced in the mantle will be sufficient to cause a significant local decrease (at the sides of the sphere in

Fig. 11c) or increase (at top and bottom) in the rotation rate of mantle material around the rigid sphere. This causes deformation of the mantle into a steady-state ellipsoid shape (Figs. 4 and 11c). The local retardation and acceleration of mantle material in a steady-state ellipsoid is demonstrated by the deflection of marker lines on ellipsoids with a high aspect ratio described above (Fig. 4a). All mantle material remains within the flow separatrix, however, and cannot move away from the rigid sphere.

If the induced viscosity contrast between mantle material and matrix is small, the flow separatrix may transect the mantle (Fig. 11d). This implies, that part of the mantle is free to move away from the central rigid sphere. The result is that after a certain amount of finite strain, wings start to form which stretch away from the central sphere.

The different types of winged objects can be explained as follows. The width in the Y-direction is a function of material rheology. Two factors probably contribute to this effect: (a) in plane strain, a highly viscous object in a less viscous matrix tends to thin in the Y-direction while it stretches. This effect was predicted by Eshelby (1957) and has been confirmed for deformed conglomerates by Freeman & Lisle (1987); (b) the flow-induced stress on

the surface of the mantle reaches maximum values in the XZ section at four sites; two in the plane of the developing wing, and two furthest away from the wing at the top and bottom of the rigid object (Masuda & Ando 1988). As a result, a critical induced viscosity contrast will only be reached in small domains around these axes, resulting in narrow wings. The influence of this factor has been proven in one experiment by varying strain rate during a single experiment: changes in thickness of the shedding wing were observed. In conclusion then, it is possible to obtain information on the rheology of deforming mantles from the width of attached wings.

The symmetry of winged mantles in XZ-section clearly depends on initial mantle thickness. Figure 10 shows that δ-shape mantles form for thin mantles only. This is probably due to the fact that δ-objects can only develop if matrix material is present inside the separatrix; this can deform into the typical embayments of δ-shape objects (Fig. 11d). Meiburg & Newton (1991) give an interesting theoretical example of δ-shape structures that develop around point vortices in Kelvin–Helmholtz flow instabilities with a shrinking separatrix. Unfortunately, their analytical approach is unsuitable for non-Newtonian materials as used in this study.

The stress–strain rate curves of materials **b**, **c** and **d** transect that of PDMS (Fig. 3). This implies that an increase in shear strain in PDMS can cause a decrease in viscosity ratio towards unity which leads to the shape-sequence discussed above. During pilot experiments we observed that material **e** deforms by rigid-body rotation, even in the case of massive spheres of mantle material and at the top range of shear strains attainable in the viscometer. Figure 3 illustrates why this happens; the stress–strain rate curves for PDMS and material **e** do not intersect, and the viscosity contrast cannot be brought to a sufficiently low level to induce permanent deformation in material **e**. Therefore, a sphere of material **e** cannot be deformed in PDMS. On the other hand, material **a** forms winged mantled spheres over the complete range of attainable shear stresses in PDMS. Figure 3 shows that this can be expected since the material is actually weaker than PDMS at the range of conditions covered.

In Fig. 10 large overlaps exist between results of different experiments, especially for material **d** which has a high n value. This can be attributed to the fact that a stress gradient exists over the mantled porphyroclasts because of the cylindrical shape of the specimen chamber. Also, materials with high n value show strongly non-linear behaviour and small changes in differential stress will have a dramatic effect on the geometry of developing mantles.

CORE-DECAY AND MANTLE GEOMETRY

Our experiments do not represent the full range of mechanically possible mantled-sphere geometries; they were carried out with a rigid central sphere whose diameter remained constant during the experiment. In natural deformation, a central porphyroclast can dimin-

ish in volume due to recrystallization in the outer rim, producing new mantle material. Unfortunately, this 'core-decay' cannot be modelled with the experimental set-up that we have chosen. The experimental results of Passchier & Simpson (1986) can be used to argue how volume loss of the central object may modify the geometries observed in our experiments. Basically we stabilize or increase the ratio of mantle width to rigid core diameter during the experiment, rather than decrease it as in the experiments described above.

In the two-dimensional experiments of Passchier & Simpson (1986), a small decay rate of the rigid object with a thin passive mantle led to development of δ-shape wings, which is confirmed by our experiments. A high decay rate, however, led to development of σ-shape rather than δ-shape wings because the produced thick mantle swamps the developing embayments typical of the δ-shape. In our experiments, no real σ-shape wings were observed, but symmetric wings or asymmetric indented wings developed for spheres with wide mantles. We expect that viscous decay of the rigid core in a mantled sphere will change its three-dimensional shape as follows:

(1) the transition from permanent sphere–steady-state ellipsoid to winged mantles with decreasing induced viscosity will probably not be affected, since similar geometries were obtained for mantled and viscous spheres in our experiments (Fig. 4);

(2) the geometry of winged mantles in XZ cross-sections will be influenced; winged mantles will be more common than permanent spheres of ellipsoid shapes, and symmetric or σ-shape wings will dominate over δ-shape wings if core-decay rate is high;

(3) the three-dimensional shape of winged mantles with low viscosity contrast will not be influenced much; however, the spindle- or coiled-shape of mantles with high viscosity contrast can be expected to be less dramatic, since constriction of wings in the Y-direction is accompanied by a decrease in width of the central object. For limited core-decay, development of a coiled mantle may be followed by detachment of the wings and further behaviour as a steady-state ellipsoid. Spindle-shaped ellipsoids (Fig. 4a) may develop into 'pulsating' ellipsoids (Fig. 4b) due to core decay.

APPLICATION TO ROCKS

The deformed mantle shapes obtained in our experiments strongly resemble those of mantled porphyroclasts in deformed rocks, especially in mylonites (Hanmer & Passchier 1991). Because of the limited amount of data presently available on the rheology of materials in mylonites, some care must be taken in the use of our results to analyse natural structures. Nevertheless, the following statements seem to be appropriate.

One of the principal results of our experiments is that development of wings around a mantled porphyroclast will only occur if the separatrix of flow lies partly or

wholly within the mantle. This will only occur if the (induced) viscosity contrast between matrix and mantle is sufficiently low. For higher viscosity contrasts, a mantled porphyroclast will remain spherical or ellipsoidal without the development of wings, even up to very high strain values. Thus, the presence of wings gives specific information on the viscosity contrast of the mantle of a porphyroclast and the surrounding matrix.

If the matrix and/or mantle of a porphyroclast are non-Newtonian, the developing geometry of the mantle depends strongly on differential stress in the matrix. This means that mantled porphyroclasts are potential stress gauges. Alternatively, if differential stress is known, conclusions could be drawn about rheological properties of mantle and matrix materials from mantle geometry alone.

The presence of round or elliptical mantled porphyroclasts in thin section are not necessarily an indication of low strain; they may represent permanent sphere or steady state ellipsoid geometry at high finite strain. Alternatively they may be winged porphyroclasts which have been subject to very high strain, in which case the wings will be thinned beyond recognition or have become detached (e.g. Fig. 7h). In some of our experiments, winged objects lost their wings at shear strains exceeding $\gamma_c = 100$ by boudinage or thinning. Such an effect may be responsible for development of 'bald' porphyroclasts in mylonite that were described by Hooper & Hatcher (1988). Another possibility is that we are dealing with cross-sections through the edge of a coiled mantled sphere (Fig. 9). Elliptical mantled porphyroclasts should therefore not be used for strain analysis.

Although the presence of porphyroclasts with spherical or ellipsoidal mantles in a deformed rock is no proof for small finite strain, the presence of a single winged porphyroclasts is indicative of high strain. The coexistence of porphyroclasts with spherical, ellipsoidal, δ-shape and symmetric mantles can be expected in mylonites which have undergone high finite strain. It may be an effect of strain-rate partitioning in the matrix, differences in initial mantle thickness or small differences in mantle rheology.

Symmetric winged mantles in XZ-section are not necessarily an effect of coaxial progressive deformation, as suggested by Passchier (1988). In our experiments approximately symmetric winged mantled spheres were formed in non-coaxial deformation if mantles were relatively wide, even at shear strains exceeding $\gamma = 100$ (Figs. 7d & j). In natural shear zones, symmetric mantled spheres in XZ-section may be an effect of initially wide mantles or rapid core decay.

If the three-dimensional shape of a winged mantle is asymmetric, XZ-sections will give the same geometry irrespective of the wing shape. XZ-sections are therefore reliable sections to determine shear sense. Although XZ-sections are important to determine shear sense, sections in the YZ-plane may show in such cases whether a mantled porphyroclast is coiled, sheathed or ridged and can thereby give an indication of the rheology

contrast between mantle and matrix, provided that flow was a plane strain (Fig. 9).

CONCLUSIONS

(1) Four main types of geometry class can develop in a mantled sphere; permanent sphere, steady-state ellipsoid, transient geometries and winged mantles.

(2) The geometry class of a deforming mantled sphere is determined by the induced viscosity contrast between mantle and matrix, which depends on stresses exerted on the surface of the mantle by the matrix material that flows around it.

(3) Finite strain only affects the geometry of transient and winged mantle shapes.

(4) Wing width in the Y-direction is a function of mantle rheology.

(5) Wings boudinage only in the case of materials with an n value exceeding 1.

(6) Symmetric winged porphyroclasts can form in simple shear flow as a response to initially wide mantles and need not be an indication for pure shear flow.

(7) The presence of round or elliptical mantled porphyroclasts in thin section are not necessarily an indication of low strain.

REFERENCES

Bentley, B. J. & Leal, L. G. 1986. An experimental investigation of drop deformation and breakup in steady, two dimensional linear flow. *J. Fluid Mech.* **167**, 241–283.

Carter, N. L. 1975. High-temperature flow of rocks. *Rev. Geophys. & Space Phys.* **13**, 344–349.

Carter, N. L. 1976. Steady state flow of rocks. *Rev. Geophys. & Space Phys.* **14**, 301–360.

Eshelby, J. D. 1957. The determination of the elastic field of an ellipsoidal inclusion, and related problems. *Proc. R. Soc. Lond.* **A241**, 376–396.

Freeman, B. & Lisle, R. J. 1987. The relationship between tectonic strain and the three-dimensional shape fabrics of pebbles in deformed conglomerates. *J. geol. Soc. Lond.* **144**, 635–639.

Ghosh, S. K. & Ramberg, H. 1976. Reorientation of inclusions by combination of pure and simple shear. *Tectonophysics* **34**, 1–70.

Hailemariam, H. Viscosity measurements of three different types of silicone putty by a co-axial cylinder viscometer. C-thesis. Internal Report, Uppsala University, Uppsala.

Hanmer, S. & Passchier, C. W. 1991. Shear-sense indicators: a review. *Geol. Surv. Pap. Can.* **90-17**.

Hooper, R. J. & Hatcher, R. D. 1988. Mylonites from the Towaliga fault zone, central Georgia: products of heterogeneous non-coaxial deformation. *Tectonophysics* **152**, 1–17.

Jeffery, G. B. 1923. The motion of ellipsoidal particles immersed in a viscous fluid. *Proc. R. Soc. Lond.* **A102**, 161–179.

Kirby, S. M. 1983. Rheology of the lithosphere. *Rev. Geophys. & Space Phys.* **21**, 1458–1487.

Koyi, H. 1988. Experimental modeling of role of gravity and lateral shortening in Zagros mountain belt. *Bull. Am. Ass. Petrol. Geol.* **72**, 1381–1394.

Kundu, P. K. 1990. *Fluid Mechanics.* Academic Press, San Diego.

Masuda, T. & Ando, S. 1988. Viscous flow around a rigid spherical body: a hydrodynamic approach. *Tectonophysics* **148**, 337–346.

McClay, K. R. 1976. The rheology of plasticine. *Tectonophysics* **33**, T7–T15.

Meiburg, E. & Newton, P. K. 1991. Particle dynamics and mixing in a viscously decaying shear layer. *J. Fluid. Mech.* **227**, 211–244.

Onogi, S. & Matsumoto, T. 1981. Rheological properties of polymer solutions and melts containing suspended particles. *Polym. Engng Rev.* **1**, 45–87.

Ottino, J. M. 1989. *The Kinematics of Mixing: Stretching, Chaos and Transport.* Cambridge University Press, Cambridge.

Passchier, C. W. 1987. Stable positions of rigid objects in non-coaxial flow—a study in vorticity analysis. *J. Struct. Geol.* **9**, 679–690.

Passchier, C. W. 1988. Analysis of deformation paths in shear zones. *Geol. Rdsch.* **77**, 309–318.

Passchier, C. W. & Simpson, C. 1986. Porphyroclast systems as kinematic indicators. *J. Struct. Geol.* **8**, 831–843.

Pffifner, O. A. & Ramsay, J. G. 1982. Constraints on geological strain rates, arguments from finite strain states of naturally deformed rocks. *J. geophys. Res.* **87**, 311–321.

Rallison, J. M. 1984. The deformation of small viscous drops and bubbles in shear flows. *Ann. Fluid Mech.* **16**, 45–66.

Ramberg, H. 1975. Particle paths, displacement and progressive strain applicable to rocks. *Tectonophysics* **28**, 1173–1187.

Smith, R. B. 1977. Formation of folds, boudinage and mullions in non-Newtonian materials. *Bull. geol. Soc. Am.* **88**, 312–320.

Taylor, G. I. 1934. The formation of emulsions in definable fields of flow. *Proc. R. Soc. Lond.* **A146**, 501–523.

Treagus, S. H. & Sokoutis, D. 1992. Laboratory modelling of strain variation across rheological boundaries. *J. Struct. Geol.* **14**, 405–424.

Tullis, J. A. 1979. High temperature deformation of rocks and minerals. *Rev. Geophys. & Space Phys.* **17**, 1137–1154.

Tullis, J. A. & Yund, R. A. 1985. Dynamic recrystallisation of feldspar: a mechanism for ductile shear zone formation. *Geology* **13**, 238–241.

Van Den Driessche, J. 1986. Structures d'enroulement et sens de cisaillement. *C.r. Acad. Sci., Paris* **303**, 413–418.

Van Den Driessche, J. & Brun, J. P. 1987. Rolling Structures at large shear strain. *J. Struct. Geol.* **9**, 691–704.

Vissers, R. L. M., Drury, M. R., Hoogerduyn Strating, E. H. & van der Wal, D. 1991. Shear zones in the upper mantle—a case study in an Alpine lherzolite massif. *Geology* **19**, 990–993.

Weijermars, R. 1986a. Flow behaviour and physical chemistry of bouncing putties and related polymers in view of tectonic laboratory applications. *Tectonophysics* **124**, 325–358.

Weijermars, R. 1986b. Polydimethyloxane flow defined for experiments in fluid dynamics. *Appl. Phys. Lett.* **48**, 109–111.

Weijermars, R. 1986c. Finite strain of laminar flows can be visualized in SGM 36-polymer. *Naturwissenschaften* **73**, 33.

APPENDIX

Table A1. List of parameters

Symbol	Definition	Dimensions
τ_a	= shear stress on inner cylinder	$[MT^{-2}L^{-1}]$
τ_r	= shear stress in PDMS at radius r	$[MT^{-2}L^{-1}]$
τ_i	= shear stress in PDMS at inner apex of mantled sphere	$[MT^{-2}L^{-1}]$
τ_e	= shear stress in PDMS at outer apex of mantled sphere	$[MT^{-2}L^{-1}]$
r	= radial distance from central axis	$[L]$
a	= radius inner cylinder	$[L]$
b	= radius inside of outer cylinder	$[L]$
D	= radius of drum on inner cylinder	$[L]$
d	= diameter of mantled sphere	$[L]$
W	= weight suspended from drum on inner cylinder	$[M]$
m'	= resistance in machine	$[M]$
Ω	= angular velocity of inner cylinder in rad s^{-1}	$[T^{-1}]$
ω_r	= angular velocity of particle at radius r	$[T^{-1}]$
$\dot{\gamma}$	= shear strain rate	$[T^{-1}]$
γ_c	= bulk shear strain in the viscometer*	$[—]$
R	= aspect ratio of deformed mantles	$[—]$

* Shear strain in the viscometer γ_c is expressed as the ratio of displacement measured along the outer cylinder and the width of the specimen chamber.